Hindawi Publishing Corporation
Journal of Nanomaterials
Volume 2013, Article ID 980390, 6 pages
http://dx.doi.org/10.1155/2013/980390

*Research Article*

# Investigation of $Fe_2O_3/SiO_2$ Nanocomposite by FESEM and TEM

**B. C. Ang,[1] I. I. Yaacob,[2] and Irwan Nurdin[1]**

[1] *Department of Mechanical Engineering, Faculty of Engineering, University of Malaya, Lembah Pantai, 50603 Kuala Lumpur, Malaysia*
[2] *Department of Manufacturing and Materials Engineering, Kulliyyah of Engineering, International Islamic University Malaysia, P.O. Box 10, 50728 Kuala Lumpur, Malaysia*

Correspondence should be addressed to B. C. Ang; amelynang@um.edu.my

Received 10 January 2013; Revised 11 March 2013; Accepted 11 March 2013

Academic Editor: Christian Brosseau



Superparamagnetic maghemite nanoparticles were synthesized using Massart's procedure. Nanocomposites that consist of the synthesized maghemite nanoparticles and silica were produced by dispersing the as-synthesized maghemite nanoparticles into the silica xerogel prepared by sol-gel technique. The system was then heated for 3 days at 140°C. The structure, morphology, and texture of the system were analysed by FESEM and TEM. The result from FESEM showed that the silica gel forms a network structure, which contained numerous pores, with an average pore size of 15 nm. EDX line profile analysis was carried out, and the result indicated that the embedded particles were iron oxide. EELS showed the presence of Fe-$L_2$ signal, which confirmed the presence of iron oxide particles within the silica matrix. The average diameters were 5.0 nm for as-synthesized maghemite nanoparticles and 4.4 nm for the embedded maghemite nanoparticles in silica xerogel matrix. The embedded maghemite nanoparticles in nanocomposite also showed a narrower distribution compared to as-synthesized particles. The magnetization values at 10 kOe applied field, $Ms_{10\,kOe}$, were 9.53 emu/g and 1.79 emu/g for as-synthesized and embedded nanoparticles, respectively. A reduction in average crystallite size was observed for the dispersed maghemite particles after formation of the nanocomposite indicating a slight dissolution of maghemite nanoparticles in silica gel.

## 1. Introduction

Maghemite is a technologically important magnetic material which has a wide range of applications in information storage [1, 2] and catalysis [3]. Nanocrystalline maghemites, in particular, have gained much interest due to their magnetic properties, which are strongly dependent on particle and crystallite sizes. This is especially so when the particle size reaches nanometre scale [4]. However, it is very difficult to prevent unwanted crystallite coarsening and particle aggregation. To overcome these problems, several attempts have been made to disperse maghemite nanoparticles in various matrix materials such as silica [5, 6], porous glass [7], and polymer [8, 9].

In this research, agglomeration and aggregation of maghemite nanoparticles are controlled by dispersing them within silica xerogel matrix. Silica xerogel is a mesoporous material, which appears in the form of an amorphous gel and is normally prepared by sol-gel polymerization. Silica xerogel consists of a three-dimensional network of $SiO_2$, which makes it highly porous. Furthermore, most of the physical size of pores is small [10]. High thermal stability [11] and biocompatibility [12] are other advantages of silica xerogel, which makes it attractive for catalytic and bioapplications.

The generation of maghemite nanocomposites can be classified into 1-step procedure and 2-step procedure. In 1-step procedure, maghemite nanocomposite is produced in a single step where maghemite nanoparticles and silica gel are produced simultaneously. In this procedure, various methods are used such as microemulsion [13–15], sol-gel [16], arc-discharge [17], reactor [18], and low-pressure flames [19].

In 2-step procedure, maghemite nanoparticles or silica gels are produced first and the encapsulation process is performed later. The 2-step procedures are used by Mornet

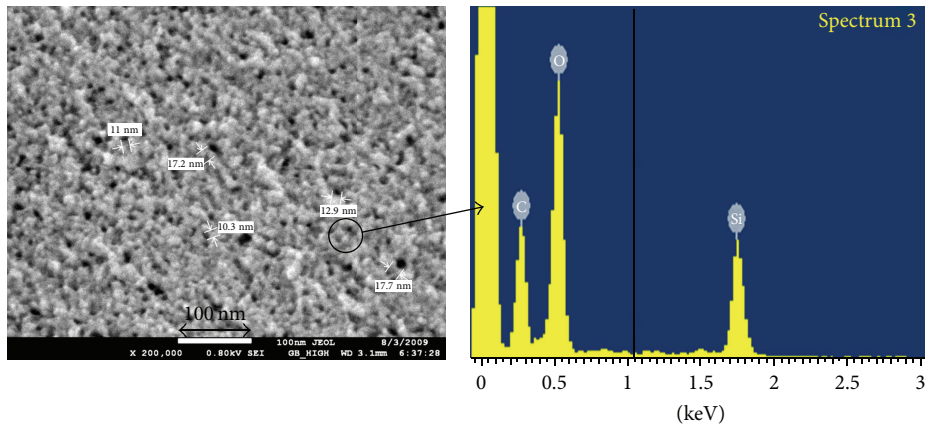


Figure 1: (a) FESEM micrograph for S1 and (b) EDX result for a specific spot on S1.

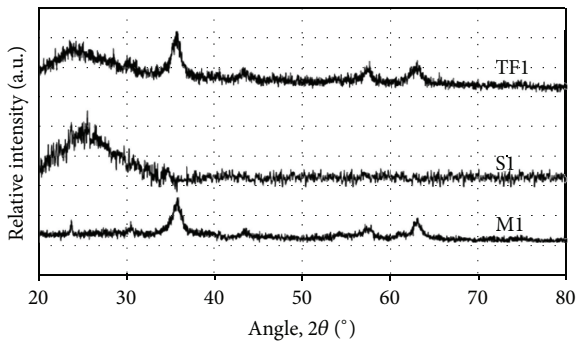


Figure 2: XRD patterns for M1, S1, and TF1.

et al. [20], Sartoratto et al. [21], and Zhang et al. [22] for producing iron oxide nanocomposites.

Although the 1-step procedure is more common compared to the 2-step procedure, the former method suffers from a major disadvantage, which is that the size and shape of the nanoparticles are difficult to control. In addition, 1-step procedure usually used surfactants, reactors, or stabilizers to help the dispersion process. It is known that such chemicals could not be completely removed [13] and the products are therefore unsuitable for bio applications.

In this research, 2-step procedure was employed without the use of a surfactant. Maghemite nanoparticles are produced by Massart's procedure and are then dispersed in silica matrix.

## 2. Sample Preparation

The raw chemicals used for preparation of maghemite nanoparticles were ferrous chloride hexahydrate (Sigma), ammonium hydroxide (Fisher Chemicals), ferric chloride (Fisher Chemicals), ferric nitrate (AJAX Chemicals), hydrochloric acid (AJAX Chemicals), and nitric acid (Merck). The raw materials used for silica xerogel were tetrapropylammonium hydroxide solution, TPA (Aldrich), and tetraethyl orthosilicate, TEOS (Aldrich). Deionized water with a resistivity of approximately 16–18 MΩ/cm was obtained using ELGA ultra-analytic deionizer and was used for the preparation of the solutions. All chemicals were of analytical grade and were used without any further purification.

Three different samples were produced in this research, namely, as-synthesized superparamagnetic maghemite nanoparticles by Massart's procedure [7], pure silica xerogel, and iron oxides-silica nanocomposite. These samples are labelled as M1, S1, and TF1, respectively. For S1, a typical sol-gel precursor mixture was prepared, using TEOS, TPA and deionized water with a weight ratio of 5 : 7 : 3. The mixture was stirred overnight and heated continuously for 3 days at 140°C. For TF1, a mixture of TEOS, TPA, and deionized water with the same weight ratio of S1 was prepared and stirred for 10 hours until a viscous gel was formed. It was then followed by adding M1 in the aged sol-gel mixture by stirring for an additional period of 3 hours. The system was heated continuously for 3 days at 140°C. The weight ratio of $Fe_2O_3/SiO_2$ remained at 0.35.

## 3. Characterization

Transmission Electron Microscope (TEM) micrographs and Electron Energy Loss Spectroscopy (EELS) were recorded on a Leo LIBRA microscope, operated at 120 kV. The samples were ground into powders using agate mortar and dispersed in deionized water. Further dispersion process was done using an ultrasonic bath. A drop of the suspension was placed onto a conventional carbon-coated copper grid for observations. The average physical size and size distribution histogram were calculated by counting roughly 100 particles. The surface texture and morphology of the samples were studied using Field Emission Scanning Electron Microscope (FESEM), Carl Zeiss Supra 55VP, and JEOL JSM-7600F. The average pore size of the silica gel was determined from about

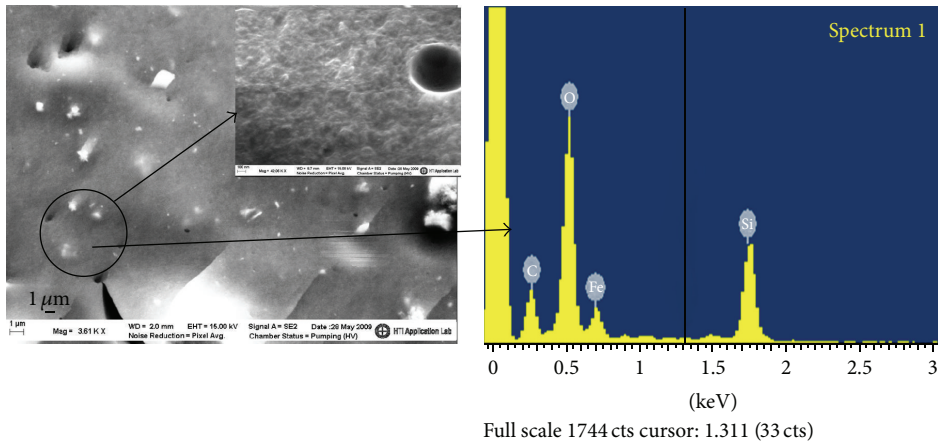


(a) (b)

Figure 3: (a) FESEM micrograph for TF1 and (b) EDX result for a specific spot on TF1.

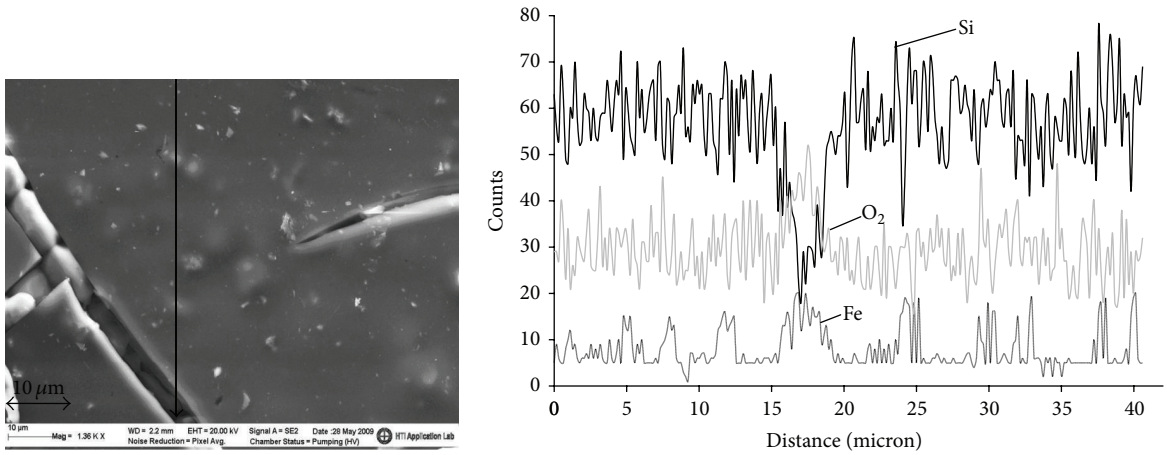


(a) (b)

Figure 4: FESEM micrograph and EDS analysis of TF1.

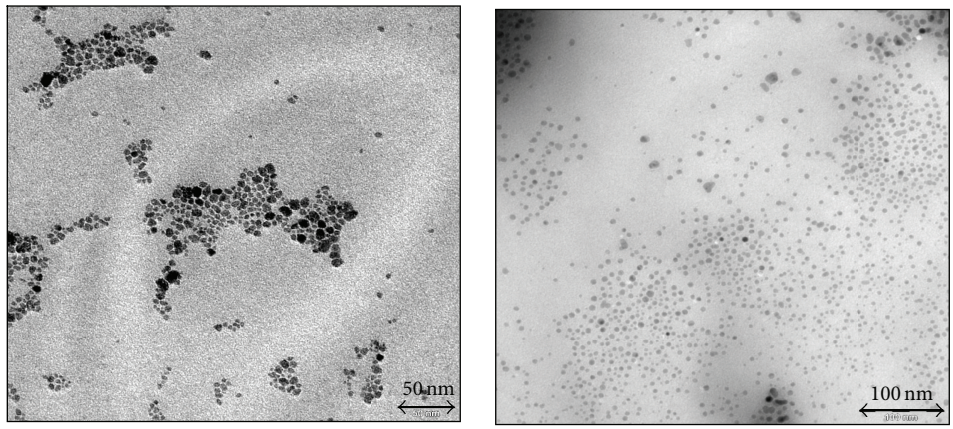


(a) (b)

Figure 5: TEM micrograph for (a) M1 and (b) TF1 in bright field mode.

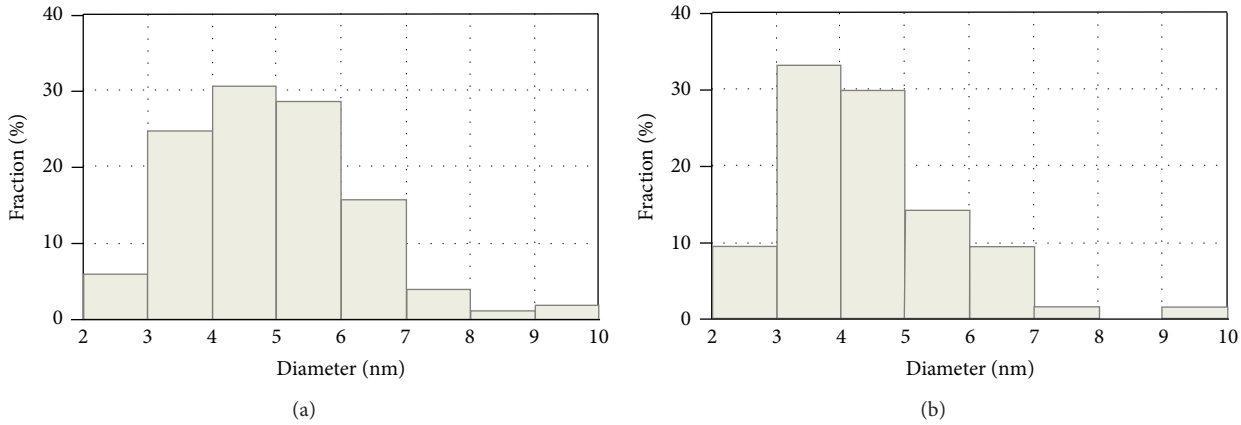


Figure 6: Size distribution histogram for (a) M1 and (b) TF1.

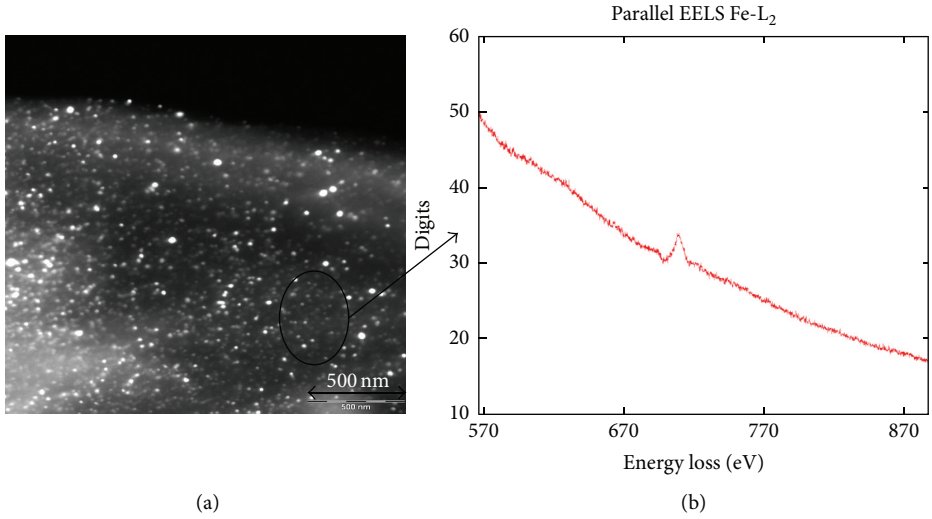


Figure 7: (a) TEM micrograph for TF1 in dark field mode and (b) EELS graph for a specific spot on TF1.

100 pores. EDX patterns were obtained using Oxford EDX system. The samples were not coated during the viewing process. To minimise charging, observation was done in a very low kV and with the help of charge compensator. The magnetic properties of the samples were measured using an Alternating Gradient Magnetometer (MicroMag, model 2900), with maximum applied fields of ±10 kOe at room temperature.

## 4. Results and Discussion

Figure 1(a) is a field emission scanning electron micrograph of silica gel (S1), which shows surface morphology of S1. The gel is in a network texture with pores. The average physical pore size is approximately 15 nm. From Figure 1(b), EDX result shows that only Si and O were present.

Figure 2 shows X-ray diffraction pattern of M1, S1, and TF1. All the peaks in M1 match well with JCPDS card, no. 39-1346. XRD pattern of S1 shows only one broad diffraction shoulder at $2\theta$ angles between 20° and 35°. This corresponds to the pattern of amorphous silica gel [18]. For samples TF1, the diffraction patterns show a broad shoulder of the silica gel and crystalline peaks, which come from the maghemite nanoparticles. The patterns show the presence of only maghemite and $SiO_2$. This indicates that there is no chemical reaction between the silica gel and the maghemite nanoparticles to form other compounds.

The surface morphology changes after incorporation of maghemite nanoparticles (Figure 3). The presence of pores is not observed in the micrograph, although the same magnification was used as sample S1. Thus, it is safe to assume that most of the pores are filled with maghemite nanoparticles. This is further proven by the EDX result in Figure 3(b), which shows that only Si, O, and Fe are present. The intensity of the Fe signal is lower, which is attributed to the fact that most of the maghemite nanoparticles are embedded within the silica gel and not on the surface. It can also be observed that some of the maghemite nanoparticles form agglomerates on the surface.

The measured average physical pore size diameter is about 15 nm, whereas the average physical size of maghemite nanoparticles is about 5.0 nm, as reported by Ang and

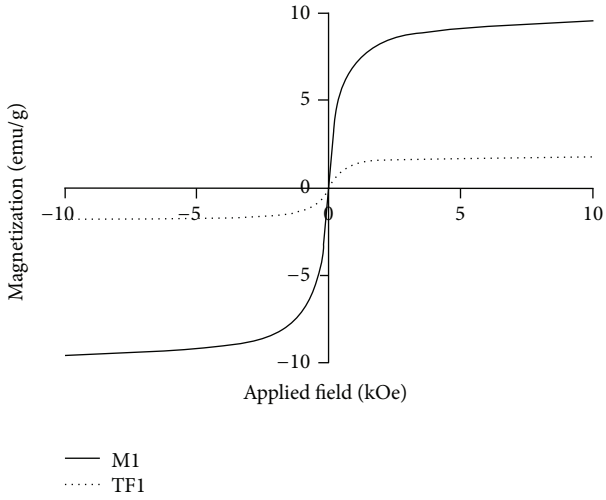


Figure 8: Magnetization curves for M1 and TF1.

Yaacob [23]. The size of the pores is nearly three times the size of the maghemite nanoparticles. This enabled the nanoparticles to fill the pores easily during the mixing process. The additional 3 hours of stirring is sufficient to form the silica network surrounding the nanoparticles, which hinders further agglomeration caused by magnetic dipole-dipole attraction among the nanoparticles. This is further proven by comparing the change in surface morphology of the samples as shown in Figures 1 and 3. The surface morphology transforms from a network with pores to a smooth continuous texture. Figure 4 shows the distribution of the dispersed maghemite nanoparticles within the silica matrix. The result shows that the maghemite nanoparticles are distributed evenly throughout the matrix. This distribution is much better as compared to the sample produced by Santra and Yang [13, 14].

Figure 5 shows TEM images of the samples. Figure 5(a) shows that the particles in sample M1 are spherical and aggregated, which may be due to the long-range magnetic dipole-dipole interaction between the particles. The observation may also be caused by the drying process during TEM sample preparation. The particle size distribution is between 1 and 9 nm, with an average diameter of 4.98 nm, as shown in Figure 6(a).

Figure 5(b) is a TEM micrograph (BF) for sample TF1. It shows dispersion of isolated nanoparticles. Figure 7(a) (DF) indicates that most of the nanoparticles are homogeneously dispersed in the silica matrix. Figure 6(b) shows size distribution histogram for TF1. It shows that TF1 has a narrower size distribution and a smaller average diameter as compared to M1. The measured average diameter for TF1 is 4.40 nm, which may be attributed to slight dissolution of $Fe_2O_3$ in the silica matrix. TEM observations using dark field mode (Figure 6(a)) reveal that the nanoparticles are distributed randomly within the silica matrix, without massive aggregation. EELS result shows the presence of Fe-$L_2$ signal and proves that the particles are iron compound.

Figure 8 shows typical hysteresis curves for samples M1 and TF1 at room temperature. The curves do not exhibit hysteresis and pass through the origin. Remanent magnetization and coercivity are not observed, which indicate that the samples are superparamagnetic. The magnetization values at 10 kOe applied field ($Ms_{10\,kOe}$) are 9.53 emu/g and 1.79 emu/g for samples M1 and TF1, respectively. The reduction in magnetization is basically due to the presence of silica, which caused an increase in total weight of the system.

The lower saturation magnetization value for M1 in comparison to multidomain bulk value of maghemite (74 emu/g) is attributed to surface effects caused by finite-size scaling of nanocrystallites. This leads to noncollinearity of magnetic moments on their surface [24].

The least upper bound of the "magnetic" size for the samples can be calculated using the saturation magnetization ($M_s$) and density of bulk maghemite, which are 74 emu/g and $5.07 \times 10^6$ g/m$^3$, respectively [25]. The least upper bound of the "magnetic" sizes is 5.92 nm for M1 and 3.01 nm for TF1. These values are comparable and in a good agreement with XRD crystallite sizes and TEM physical sizes.

## 5. Conclusion

$Fe_2O_3/SiO_2$ nanocomposite was successfully produced using sol-gel technique. The FESEM micrograph clearly showed that most of the maghemite nanoparticles were embedded into the pores of the silica matrix. Measurements of the physical size of maghemite nanoparticles using TEM showed that the encapsulated maghemite nanoparticles had a finer average diameter. The EDS and TEM results revealed that the maghemite nanoparticles were distributed evenly within the matrix. This indicated that silica matrix functioned as a physical barrier to prevent agglomeration and aggregation of maghemite nanoparticles. Slight dissolution of maghemite nanoparticles was observed in the silica matrix. The nanocomposites show superparamagnetic behaviour, which showed that the presence of the silica matrix did not affect the behaviour of the embedded maghemite nanoparticles.

## Acknowledgment

This work is partially funded by the University of Malaya under the UMRG Fund, Project no. RP021-2012C.

## References

[1] M. Sugimoto, "The past, present and future of ferrites," *Journal of the American Ceramic Society*, vol. 82, pp. 269–280, 1999.

[2] G. Bate, "Magnetic recording materials since 1975," *Journal of Magnetism and Magnetic Materials*, vol. 100, pp. 413–424, 1999.

[3] T. Ida, H. Tsuiki, A. Ueno et al., "Characterization of iron oxide in $Fe_2O_3$ $SiO_2$ catalyst," *Journal of Catalysis*, vol. 106, no. 2, pp. 428–439, 1987.

[4] M. P. Morales, C. Pecharroman, T. G. Carreñ, and C. J. Serna, "Structural characteristics of uniform $\gamma$-$Fe_2O_3$ particles with different axial (length/width) ratios," *Journal of Solid State Chemistry*, vol. 108, no. 1, pp. 158–163, 1994.

[5] G. Ennas, A. Musinu, G. Piccaluga et al., "Characterization of iron oxide nanoparticles in an $Fe_2O_3$-$SiO_2$ composite prepared by a sol-gel method," *Chemistry of Materials*, vol. 10, pp. 495–502, 1998.

[6] F. Del Monte, M. P. Morales, D. Levy et al., "Formation of $\gamma$-$Fe_2O_3$ isolated nanoparticles in a silica matrix," *Langmuir*, vol. 13, no. 14, pp. 3627–3634, 1997.

[7] N. F. Borelli, D. L. Morse, and J. W. H. Schreurs, "Magnetic properties of iron oxide photolytically produced from $Fe(CO)_5$ impregnated porous glass," *Journal of Applied Physics*, vol. 54, no. 6, article 3344, 7 pages, 1983.

[8] R. F. Ziolo, E. P. Giannelis, B. A. Weinstein et al., "Matrix-mediated synthesis of nanocrystalline $\gamma$-$Fe_2O_3$: a new optically transparent magnetic material," *Science*, vol. 257, no. 5067, pp. 219–223, 1992.

[9] M. T. Nguyen and A. F. Diaz, "A novel method for the preparation of magnetic nanoparticles in a polypyrrole powder," *Advanced Materials*, vol. 6, no. 11, pp. 858–860, 1994.

[10] H. Hirashima, C. Kojima, K. Kohama et al., "Oxide aerogel catalysts," *Journal of Non-Crystalline Solids*, vol. 225, no. 1–3, pp. 153–156, 1998.

[11] L. M. Hair, P. R. Coronado, and J. G. Reynolds, "Mixed-metal oxide aerogels for oxidation of volatile organic compounds," *Journal of Non-Crystalline Solids*, vol. 270, no. 1–3, pp. 115–122, 2000.

[12] L. Casas, A. Roig, E. Rodríguez, E. Molins, J. Tejada, and J. Sort, "Silica aerogel-iron oxide nanocomposites: structural and magnetic properties," *Journal of Non-Crystalline Solids*, vol. 285, no. 1–3, pp. 37–43, 2001.

[13] S. Santra, R. Tapec, N. Theodoropoulou, J. Dobson, A. Hebard, and W. Tan, "Synthesis and characterization of silica-coated iron oxide nanoparticles in microemulsion: the effect of nonionic surfactants," *Langmuir*, vol. 17, no. 10, pp. 2900–2906, 2001.

[14] H. H. Yang, S. Q. Zhang, X. L. Chen, Z. X. Zhuang, J. G. Xu, and X. R. Wang, "Magnetite-containing spherical silica nanoparticles for biocatalysis and bioseparations," *Analytical Chemistry*, vol. 76, no. 1, pp. 1316–1321, 2005.

[15] M. F. Casula, A. Corrias, and G. Paschina, "Iron oxide-silica aerogel and xerogel nanocomposite materials," *Journal of Non-Crystalline Solids*, vol. 293–295, no. 1, pp. 25–31, 2001.

[16] C. Cannas, G. Concas, D. Gatteschi et al., "Superparamagnetic behaviour of $\gamma$-$Fe_2O_3$ nanoparticles dispersed in a silica matrix," *Physical Chemistry Chemical Physics*, vol. 3, no. 5, pp. 832–838, 2001.

[17] R. Fernández-Pacheco, M. Arruebo, C. Marquina, R. Ibarra, J. Arbiol, and J. Santamaría, "Highly magnetic silica-coated iron nanoparticles prepared by the arc-discharge method," *Nanotechnology*, vol. 17, no. 5, pp. 1188–1192, 2006.

[18] E. Barrado, J. A. Rodríguez, F. Prieto, and J. Medina, "Characterization of iron oxides embedded in silica gel obtained by two different methods," *Journal of Non-Crystalline Solids*, vol. 351, no. 10-11, pp. 906–914, 2005.

[19] C. Janzen, J. Knipping, B. Rellinghaus, and P. Roth, "Formation of silica-embedded iron-oxide nanoparticles in low-pressure flames," *Journal of Nanoparticle Research*, vol. 5, no. 5-6, pp. 589–596, 2003.

[20] S. Mornet, F. Grasset, J. Portier, and E. Duguet, "Maghemite@silica nanoparticles for biological applications," *European Cells and Materials*, vol. 3, no. 2, pp. 110–113, 2002.

[21] P. P. C. Sartoratto, K. L. Caiado, R. C. Pedroza, S. W. da Silva, and P. C. Morais, "The thermal stability of maghemite-silica nanocomposites: an investigation using X-ray diffraction and Raman spectroscopy," *Journal of Alloys and Compounds*, vol. 434-435, pp. 650–654, 2007.

[22] L. Zhang, G. C. Papaefthymiou, R. F. Ziolo, and J. Y. Ying, "Novel $\gamma$-$Fe_2O_3$/$SiO_2$ magnetic nanocomposites via sol-gel matrix-mediated synthesis," *Nanostructured Materials*, vol. 9, no. 1–8, pp. 185–188, 1997.

[23] B. C. Ang and I. I. Yaacob, "Preparation of maghemite-silica nanocomposites using sol-gel technique," *Advanced Materials Research*, vol. 97–101, pp. 2140–2143, 2010.

[24] S. Gubbala, H. Nathani, K. Koizol, and R. D. K. Misra, "Magnetic properties of nanocrystalline Ni-Zn, Zn-Mn, and Ni-Mn ferrites synthesized by reverse micelle technique," *Physica B*, vol. 348, no. 1–4, pp. 317–328, 2004.

[25] A. B. Chin and I. I. Yaacob, "Synthesis and characterization of magnetic iron oxide nanoparticles via w/o microemulsion and Massart's procedure," *Journal of Materials Processing Technology*, vol. 191, no. 1–3, pp. 235–237, 2007.